Investigation of low-zinc-solubility electrodes and electrolytes in zinc/silver oxide cells

Jenn-Shing Chen*, Frank R. McLarnon and Elton J. Cairns
Energy & Environment Division, Lawrence Berkeley Laboratory and Department of Chemical Engineering, University of California, Berkeley, CA 94720 (USA)

(Received February 25, 1992; in revised form April 6, 1992)

Abstract

The cycle-life performance of the Zn/AgO cell is limited by high rates of Zn active material redistribution (shape change) and Zn dendrite growth. Reduced-zinc-solubility electrolytes, prepared by adding F^-, CO_3^{2-}, BO_3^{3-} and PO_4^{3-} salts to aqueous KOH solutions, were used in 5 A h Zn/AgO cells to determine their effect on cell lifetimes. $Ca(OH)_2$ additions to the Zn electrode were also evaluated in cells of the same capacity and mass as the calcium-free cells. It was found that all of the anion additives to KOH electrolytes resulted in lower cell capacities and shorter lifetimes, which could be attributed the formation of soluble Ag-containing salts and subsequent degradation of the Ag electrode performance. The calcium-containing Zn electrode was found to significantly improve the performance of the Zn/AgO cell by promoting higher capacities, especially over the initial 20 cycles. The higher capacities could be attributed to the formation of a calcium zincate complex, crystals of which were found in the cycled Zn electrodes.

Introduction

The general advantages of Zn/AgO batteries are high specific energy, high discharge rate capability, good charge acceptance, and low self-discharge rate. However, the principal disadvantages of high cost and short cycle life have limited the use of this battery to applications where high specific energy is the prime requisite, such as military and flight applications, portable electronic equipment, etc. There exists a strong incentive to improve the Zn/AgO cell cycle life and increase its performance; in order to reduce battery cycle-life costs and thereby widen the range of applications. The redistribution of Zn-active material (shape change) and the growth of Zn dendrites (which leads to cell shorting) have been identified as primary factors that limit the cycle-life performance of Zn/AgO cells. These phenomena can be partly overcome by improvements in separator materials, and by additives to the electrode and electrolyte. Recent development work on Zn/AgO cells has been concentrated in the area of Zn electrode and separator improvements to extend the lifetimes of cells [1, 2]. It is well known that shape change and dendrite problems can be attributed to the high solubility of the ZnO discharge product in concentrated KOH electrolyte. Because the ZnO solubility depends strongly on the KOH concentration, a useful strategy is to operate the cell

*Current address: Industrial Technology Research Institute, Building 64, 195 Chung Hsing Rd., Section 4, Hsinchu 31015, Taiwan R.O.C.

0378-7753/92/$5.00

at as low a KOH concentration as can be tolerated by the positive electrode, and add indifferent supporting electrolyte to maintain acceptable ionic conductivity. Much research has successfully applied different alternative electrolytes, such as those containing fluoride, borate, phosphate, arsenate, and carbonate ions, to extend Zn/NiOOH cell cycle life [3]. In this work, a primary objective was to determine the ability of reduced-zinc-solubility electrolytes to extend the cycle life of Zn/AgO cells by additives (F^-, CO_3^{2-}, BO_3^{3-}, PO_4^{3-}) to the KOH electrolyte.

Many investigations have shown that the addition of $Ca(OH)_2$ to the Zn electrode can reduce the zincate-ion ($Zn(OH)_4^{2-}$) solubility and thereby improve the cycle life of Zn/NiOOH cells [3–5]. When $Ca(OH)_2$ is added to ZnO in alkaline electrolyte, an insoluble calcium zincate compound, $Ca(OH)_2 \cdot 2Zn(OH)_2 \cdot 2H_2O$, is formed, thereby 'trapping' the soluble $K_2Zn(OH)_4$ species [6]. Therefore, in this research the other objective was to determine the ability of calcium-containing zinc electrodes to extend the cycle life of Zn/AgO cells.

Experimental procedures

Two groups of cells were tested. One group of cells was fabricated by BST, Inc. and the other group was fabricated by Lawrence Berkeley Laboratory (LBL).

Cell construction

All cells were designed to be Ag-limiting in capacity, and deliver 5 A h of rated capacity. The electrode sizes were 4.45 cm × 3.56 cm, and each cell contained six AgO electrodes, five full-capacity Zn electrodes, and two half-capacity Zn electrodes which were used as the outermost electrodes in the cell pack. Cell design calculations are presented in Table 1.

Electrode specifications

All positive electrodes used in this work were furnished by BST, Inc. Each positive electrode contained 2.58 g Ag applied on a Ag mesh current collector and was ~0.038 cm thick. In the BST-cell group, each full-capacity negative electrode contained 3.66 g ZnO applied to a Ag sheet current collector and was about 0.089 cm thick. In the LBL-cell group, the negative electrodes were prepared by a vacuum-table process [7], which is outlined in Fig. 1. Each electrode contained 3.7 g ZnO and was ~0.122 cm thick. The electrode compositions were: 93 wt.% ZnO (Mallinckrodt, Inc., Paris, KY, 99.9% pure), 2 wt.% PbO (Mallinckrodt, Inc., 99% pure), 4 wt.% polytetrafluoroethylene (PTFE) (E.I. Dupont de Nemours and Co., Wilmington, DE, Teflon Type 30 dispersion), and 1 wt.% Coronado newsprint (The Morilla Company, Los Angeles, CA). An 0.55 mm diameter Ag wire (Johnson Matthey/AESAR, Seabrook, NH) was spot-welded onto a Ag mesh current collector (Exmet Corp., Bridgeport, CT, 5Ag54-0). The Zn–Ca electrode was of the same initial mass as a full-capacity Zn electrode. Because a 25 mol.% $Ca(OH)_2$ electrode (based on the mol.% Zn and Ca in the uncycled electrode, not including inert materials) exhibited good cycle-life performance in Zn/NiOOH cells [5], this composition was selected for use in the Zn–Ca/AgO cells. The density of $Ca(OH)_2$ is 2.24 g/cm^3, which may be compared to 5.61 g/cm^3 for ZnO. Therefore the Zn–Ca electrodes occupied a greater volume and thus required more binder and led to a thicker negative electrode. The electrode was 0.170 cm thick and contained 92 wt.% ZnO + $Ca(OH)_2$, 2 wt.% PbO, 5 wt.% PTFE and 1 wt.% newsprint. The procedure for fabricating Zn–Ca electrodes was similar to that for Zn electrodes [5].

TABLE 1

Zn/AgO cell design (silver-limiting capacity design)

	BST	LBL
Rated capacity	5 A h	5 A h
Electrode size (each plate)	4.45 cm × 3.56 cm	4.45 cm × 3.56 cm
Weight of Zn or Ag/cell	ZnO = 21.96 g Ag = 15.48 g	Zn: ZnO = 22.2 g ZnCa: ZnO = 17.03 g $Ca(OH)_2$ = 5.17 g Ag = 15.48 g
Ratio of active materials	Mzn/Mag Mass Ratio = 1.14	Zn: Mzn/Mag Ratio = 1.15 Zn–Ca: Mzn/Mag Ratio = 0.88
Porosity (as metal based)	ZnO = 50–60% Ag = 55–60%	ZnO = 65–70%, Zn–Ca = 65–70% Ag = 55–60%
Cell pack	7: ZnO, 6: Ag, 12: Sep.	7: ZnO, 6: Ag, 12; Sep.
Separator system	−/Dexter//5 cp[a]/cg[b]/Pellon/+	−/2 cg[b]//5 cp/cg/Pellon/+
Thickness for each plate	ZnO = 0.089 cm (35 mils) Ag = 0.038 cm (15 mils)	ZnO = 0.122 cm (48 mils) Zn–Ca = 0.175 cm (67 mils) Ag = 0.038 cm (15 mils)
Total thickness of cell	1.453 cm (572 mils)	Zn = 1.686 cm (664 mils) Zn–Ca = 2.006 cm (790 mils)

[a]5 layers of cellophane.
[b]1 or 2 layers of Celgard.

Separator and wick

Each Ag electrode was wrapped with a layer of Pellon 2524 wicking material (Pellon Division of Freudenberg-Nonwoven Corp., Chelmsford, MA) and Celgard separator, which were provided by BST company, and five layers of cellophane as the outer separator layers. The BST-group cells used one layer of Dexter paper (The Dexter Corp., Windsor Locks, CT, Grade 10) around the Zn electrode, and the paper was sealed with cellophane tape (3M Corp., St. Paul, MN). In the LBL-group cells, two layers of Celgard 3401 (Celanese Fibers Corp., Summitt, NJ) microporous polypropylene sheet were heat-sealed around the zinc electrode.

Electrolyte preparation

Table 2 lists the compositions of the various electrolytes that were tested. In order to simplify comparisons among these electrolytes, all of them were constituted to have a similar ionic strength ($I \sim 15$–16). The standard electrolyte was 45 wt.% KOH (AnalaR grade solution, J. T. Baker Chemicals Co., Phillipsburg, NJ). The K_2CO_3 and H_3BO_3 were ACS reagent-grade chemicals (Fisher Scientific, NJ), the KF and K_3PO_4 were Baker AnalaR grade chemicals, and 15 mΩ cm or better deionized water was used. Following preparation of each solution, ZnO was added in sufficient quantity to saturate the electrolyte.

Cell assembly

The cell pack (separator/electrode) assembly was designated for split-wrap [2] configuration. The positive electrodes were wrapped in pairs and the tube thus formed

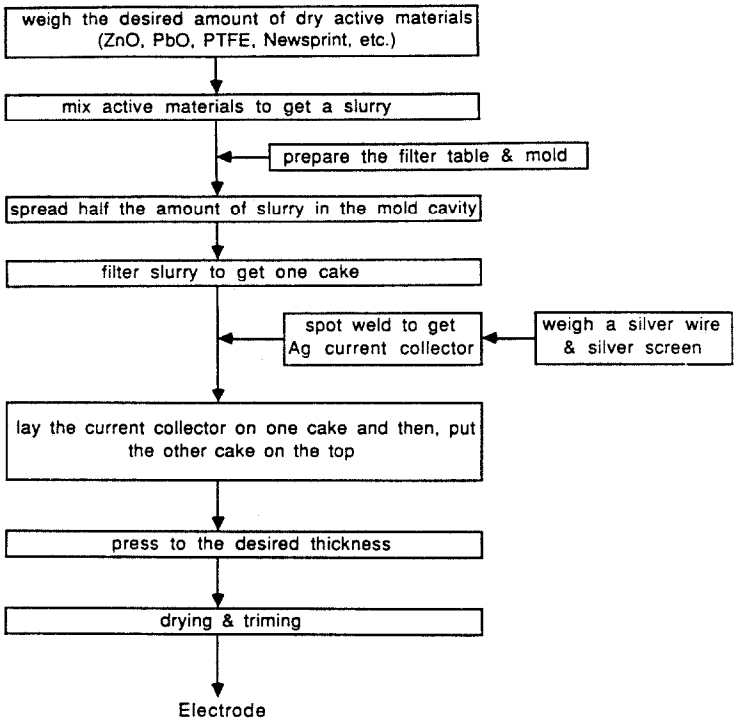

Fig. 1. Flow chart for making zinc electrodes for Zn/AgO cells.

was folded at the center line so that two electrodes were enclosed in one bag and the negative electrodes were individually bagged with the bottoms sealed. The cell cases were made from 0.18 cm thick polysulfone (for the BST-group cells) and from 0.14 cm thick acrylic (for the LBL-group cells). In order to analyze the behavior of individual electrodes, a reference electrode was used for every cell except B1 and B2. A Hg/HgO electrode located in a separate reference compartment that was filled with the same electrolyte was used as the reference electrode. The cell pack was placed in a tightly fitting cell case, and each cell was filled with 20 ml of electrolyte and allowed to stand for about 5 days. The cell was then vented through an Ascarite column to prevent CO_2 from entering the cell.

Cell cycling tests

Cells were cycled under controlled charge and discharge regimens using a combination of analog and digital equipment, which has been described in detail in ref. 8. All cells were tested at constant current. Prior to beginning regular cycle testing, two formation cycles were performed in order to render the cell active. The first formation cycle employed a 0.5 A charge to 2.2 V cell cutoff voltage, followed by a 0.5 A discharge to a 1.1 V cutoff. The second formation cycle employed a 0.5 A charge to a 2.01 V cell cutoff voltage, followed by a 0.5 A discharge to a 1.1 V cell cutoff voltage. Standard cycle testing used 0.5 A charge current to a 2.01 V cell cutoff voltage and a 1.0 A discharge current to a 1.1 V cell cutoff voltage, and an open-circuit period of 30 minutes was implemented at the end of each half-cycle.

TABLE 2

Cycle-life performance data for representative groups of 5.0 A h Zn/AgO cells

Cell[a]	Electrolyte[b]	Total No. cycles completed[c]	Final % capacity (% rated capacity)	No. cycles (Before cells reached 80% rated capacity)	% capacity loss/cycle[d]	Average A h/cycle
BST-group						
B1	$45OH^-$	136	19	134	0.19	4.85
B1(2)	$45OH^-$	65	73	59	0.47	4.79
B2	$34OH^-/3.6F^-/8.8CO_3^{-2}$	97	71	44	0.3	4.39
B3	$25.6OH^-/3.9F^-/15.9CO_3^{-2}$	70	62	29	0.63	4.17
B4	$25.2OH^-/12.4F^-/8.8CO_3^{-2}$	58	63	6	1.13	4.22
B5	$17OH^-/8F^-/19CO_3^{-2}$	5	65	0		
LBL-group (Zn)						
L1	$45OH^-$	144	75	114	0.26	4.51
L2	$37OH^-/9F^-$	45	60	10	0.29	4.30
L3	$38OH^-/8CO_3^{-2}$	151	78	60	0.38	4.30
L4	$39OH^-/5BO_3^{-3}$	94	77	53	0.52	4.34
L5	$39OH^-/6PO_4^{-3}$	21	69	0		
LBL-group (Zn–Ca)						
C1	$45OH^-$	185	56	124	0.24	4.95
C1(2)	$45OH^-$	118	75	101	0.12	4.89

[a]Separator system: BST-group: −/dexter//5 layers of cellophane/1 layer of Celgard/Pellon/+; LBL-group: −/2 layers of Celgard//5 layers of cellophane/1 layer of Celgard/Pellon/+.

[b]Anions identified common K^+ ion, all numbers in wt.%.

[c]Failure mode: B1: short; other cells: capacity loss.

[d]Calculated based on the cell capacity at the first cycle.

Analysis of cycled cells

After cells completed cycling, the Zn electrodes were examined to determine the extent of the shape charge, and each separator layer was analyzed for Ag content. Zinc electrode shape change was determined by analysis of X-ray photographs, which were obtained using a 60 KeV X-ray beam, and an exposure of 100 m A s. Scanning electron microscopy (SEM) was employed for qualitative analysis of the zinc electrode morphology. An AMR model 1000 SEM was used for this purpose. The Ag content of the separator was determined by Volhard methods [9]. Samples of the separators were cut from the electrodes, rinsed several times with distilled water, and then placed in a 250 ml beaker with 25 ml of 42 wt.% nitric acid. The beaker was heated for about 30 min to aid in the dissolution of the Ag from the separator sample. The resulting solutions were titrated with 0.1 N or 0.01 N ammonium thiocyanate (Baker AnalaR grade) using ferric ammonium sulfate (Fisher Scientific ACS grade) as an indicator. The tensile strength of the cellophane separators was measured in order to determine the effect of electrolyte composition on separator tensile strength. Measurements were made using an Instron electrohydraulic tensile tester model 1321.

Results and discussion

A total of 6 cells in the BST-cell group were subjected to cycle-life testing to evaluate standard electrolyte (as a control test for comparison purposes), and the alkaline-fluoride and alkaline-carbonate electrolytes listed in Table 2. The cell capacity data shown in Table 2 are based on the cell rated capacities, i.e. 5 A h = 100% capacity, regardless of the initial or maximum capacity exhibited by the cell. Cells B1, B1(2) and L1 with standard electrolyte were used as control cells in the BST-cell and LBL-cell groups.

Cell cycle-life performance

Figure 2 shows a plot of capacity versus cycle number for the BST-cell group. All of the cells had at least 98% coulombic efficiency for all standard cycles. However cells with additives in the electrolyte exhibited a lower capacity than the cells with standard 45 wt.% KOH electrolyte. Increasing amounts of KF added to KOH electrolyte resulted in a lower capacity than that exhibited by the control cell B1. The capacity of cell B1 reached its maximum value ($\sim$115%) after about 20 cycles, and it remained above 80% up to 135 cycles, after which it fell precipitously. This cycle-life performance behavior is better than that typical of Zn/AgO cells cycled at 100% depth-of-discharge (DOD), however the replicate cell B1(2) dropped below 80% capacity before it reached 60 cycles, which is a more typical behavior. The shapes of the discharge curves indicated that the Ag electrodes were capacity-limiting for all cells throughout testing. The lower capacities of the cells with additives can therefore be attributed to poorer behavior of the Ag electrode in the presence of the modified electrolytes. Open-circuit stand tests (to evaluate charge retention) for cell B1 were conducted at cycles 46, 47 and 103 for 84, 87 and 73 h, respectively. The cell maintained its normal coulombic efficiency ($>$98%) during these tests. However, the coulombic efficiency declined to about 92% after a 52 h open-circuit test at cycle 125, and the coulombic efficiency fell below 25% after cycle 135. The lower coulombic efficiency near the end of cell life suggests that the failure of cell B1 can be attributed to Zn dendrites (hard short). Dendrite growth was indeed observed around the negative electrodes.

Figure 3 shows capacity versus cycle number for the LBL-fabricated cells, cells L1–L5. Similar to the results with the BST-cell group, cells with different electrolyte

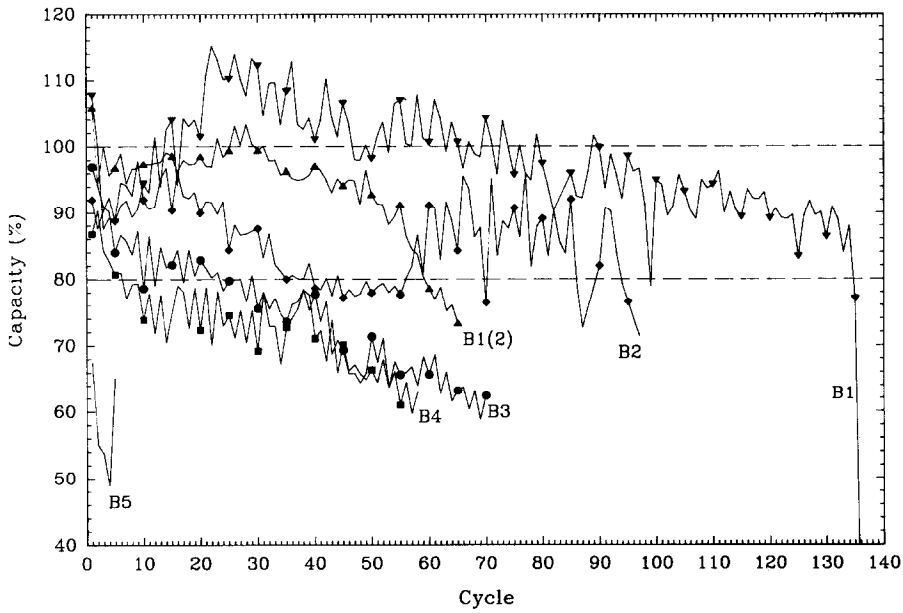

Fig. 2. Capacity vs cycle number for the BST-cell group. The electrolyte compositions (in wt.%) are listed below, and are also listed in Table 2. Note that all electrolytes were initially saturated with ZnO. B1 (▼) and B1(2) (△): 45% KOH; B2 (◆): 34% KOH, 3.6% KF and 8.8% K_2CO_3; B3 (●): 25.6% KOH, 3.9% KF and 15.9% K_2CO_3; B4 (■): 17% KOH, 8% KF and 19% K_2CO_3; B5: 25.2% KOH, 12.4% KF and 8.8% K_2CO_3.

additives (fluoride, carbonate, borate, and phosphate) showed generally lower capacities, especially those with fluoride and phosphate additives. Figure 4 shows cell voltages and electrode potentials for the control cell L1. This cell, and the other cells containing electrolyte additives, exhibited the expected shapes of charge and discharge curves, and the Ag electrode limited the capacity of all cells. The low capacities of the cells with electrolyte additives may be attributed to the formation of inorganic salts at the Ag electrode (e.g., AgF or AgF_2, $AgPO_4$, etc.) resulting in Ag-active materials loss. Control cell L1 reached 115 cycles and maintained 80% of its original capacity, which is very good performance for a cell of this type.

Calcium-containing cells

Cells L1 and C1 were filled with 45 wt.% KOH electrolyte and employed the same separator system, and differed only in the composition of the Zn electrode. However, cell C1 with $Ca(OH)_2$ in the Zn electrode showed higher capacity and longer cycle life (see Table 2), and both cells showed normal coulombic efficiencies (>98%). The total delivered capacity was 538 A h for cell L1 and 598 A h for cell C1 for the first 120 cycles, over which both of cells maintained >80% of rated capacity. This difference in performance can be attributed to the addition of $Ca(OH)_2$ to the Zn electrode, and subsequent formation of an insoluble $Ca(OH)_2 \cdot 2Zn(OH)_2 \cdot 2H_2O$ complex [6], which lowers the concentration of soluble zincate species and causes somewhat different cell behavior. Especially at higher KOH concentration, the calcium zincate decomposition rates are relatively fast [10].

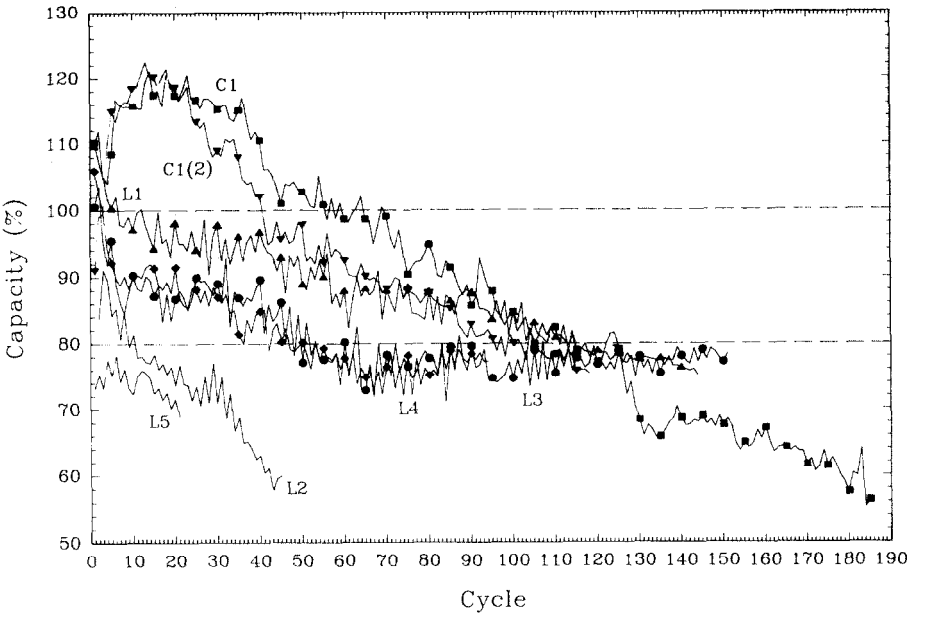

Fig. 3. Capacity vs cycle number for the LBL-cell group. The electrolyte compositions (in wt.%) are listed below, and are also listed in Table 2. Note that all electrolytes were initially saturated with ZnO. L1 (▲), C1 (■) and C1(2) (▼): 45% KOH; L2: 37% KOH and 9% KF; L3 (●): 38% KOH and 8% K_2CO_3; L4 (◆): 39% KOH and 5% K_3BO_3; L5: 39% KOH and 6% K_3PO_4.

Figure 5 shows cell voltage and electrode potentials for various cycles for cell Cl. The first charge plateau (the formation of Ag_2O) was longer than typical and became shorter with increasing cycle number. The unusually long first charge plateau results in higher capacity and lower average charge voltage. Also, the flat discharge plateau was longer than typical, and the average discharge voltage was lower. During the oxidation of Ag electrodes, the formation of Ag_2O and AgO films results in two charge plateaus, where the second charge plateau (the formation of AgO) is longer than the first one (the formation of Ag_2O). At moderate current densities, both processes are about 100% efficient [11]. Therefore, the length of the plateaus is a function of the relative thickness of the oxide films. Generally, the thickness of the film depends on the current density, electrolyte concentration, and physical state of the electrode [12]. The faster calcium zincate decomposition rate (compared to the decomposition rate of $K_2Zn(OH)_4$) in higher KOH concentration electrolytes facilities OH^- transport from the Zn electrode to the Ag electrode, and can thereby result in longer first charge plateau (or thicker Ag_2O film). However, after extended cycling, the deposition of Ag on the separator may hinder OH^- ion transport form the Zn to the Ag electrode. Also, active material loss in the electrodes results in a shorter charge plateau and lower capacity. Open-circuit stand tests (to evaluate charge retention) for cell C1 were conducted at cycles 59, 76 and 180 for 72, 48 and 58 h, respectively. The cell maintained its normal coulombic efficiency (>98%) during these tests. Unlike cell B1, cell C1 did not exhibit dendrite problems, even after 180 cycles.

Cell C1(2) was intended to replicate the long-lived and high-capacity control cell C1. Both cells had the same cell pack design, and differed only in the thickness of

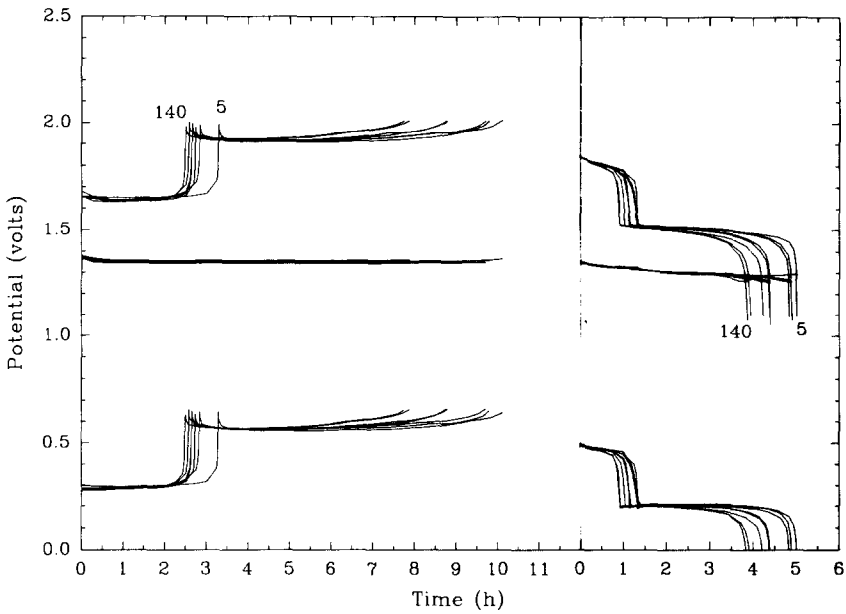

Fig. 4. Cell voltage and electrode potentials at different cycles for cell L1. Potential vs time curves are identified for cycle #5 and cycle #140, and the curves for intermediate cycles (#20, #40, #60, #80, #100, #120) are shown but not identified. The uppermost curves represent the cell voltage, the middle curves represent the negative of the Zn electrode potential (vs Hg/HgO), and the lowermost curves represent the AgO electrode potential (vs Hg/HgO). Cell charge is shown on the left-hand side, and cell discharge is shown on the right-hand side.

the respective cell cases — cell C1(2) had a 0.1 cm thicker cell case than cell C1. Both cells showed a similar maximum capacity of ~122% of the rated value between cycles 15 and 20 (see Fig. 3). Because cell C1(2) showed only 90% of rated capacity after its formation cycles, the capacity of cell C1(2) was lower than that of cell C1, however the shapes of capacity versus cycle number curves were similar.

Figure 6 shows capacity versus cycle number for cells B1, L1 and C1. All three cells were constructed in a similar manner, and the major difference among these cells is the composition and fabrication of the Zn electrodes. The Zn electrodes utilized in cell B1 were made by BST, Inc., and LBL fabricated the Zn electrodes used in cells L1 and C1. $Ca(OH)_2$ was added to the Zn electrodes only in cell C1, as described above. Also, one layer of Dexter paper was used around the Zn electrode in cell B1, whereas two layers of Celgard 3401 were used in cells L1 and C1. Dendrite problems were the cause of failure only in cell B1 (after 136 cycles). Apparently, the separator Celgard 3401 has the beneficial effect of preventing dendrite growth in these cells. Cells B1 and C1 showed comparable total delivered capacity (~656 A h) and cell L1 exhibited a somewhat lower total delivered capacity (~601 A h) up to cycle 136 when cell B1 failed. Even though cells B1 and C1 show comparable capacities, cell C1 exhibited higher capacities early in life and a longer cycle life.

Analyses of cell components

The Ag content of the separators was determined after the cells completed their cycling tests. Figure 7 shows the Ag content of the separator system for cell C1 after

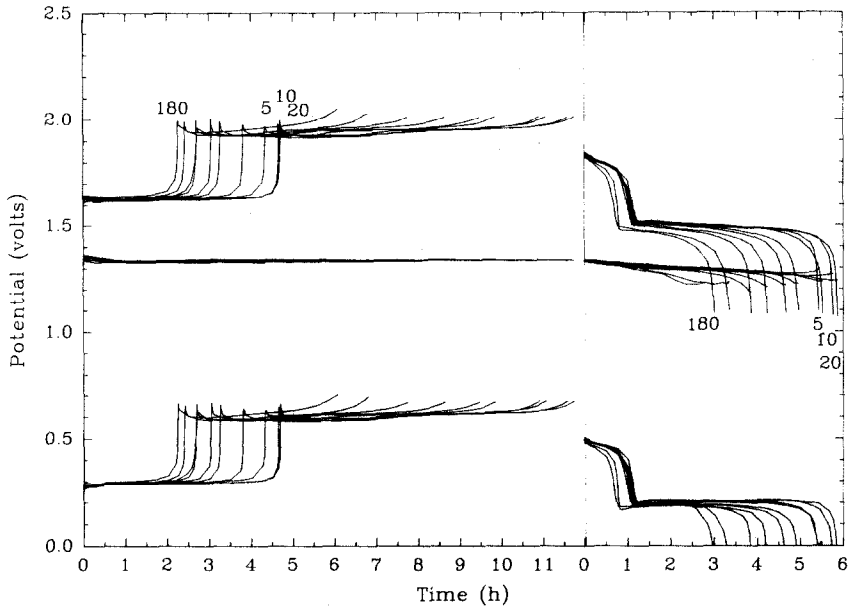

Fig. 5. Cell voltage and electrode potentials at different cycles for cell C1. Designations are the same as for Fig. 4, except that the potential vs time curves are identified for cycles #5, #10, #20 and #180, and the curves for the intermediate cycles (#40, #60, #80, #100, #120 and #160) are shown but not identified.

completing 185 cycles. The highest Ag content was found in the first layer of cellophane adjacent to the Ag electrode. Cell C1, after completing 185 cycles, showed that Ag penetration became progressively smaller through one layer of Pellon wick, one layer of Celgard and three layers of cellophane, and similar results were found for other cells. Table 3 shows the results of the tensile-strength test of cellophanes in different electrolytes for different periods of time. These results show that tensile strength decreased with lower KOH concentrations.

X-ray images of uncycled Zn and Zn–Ca electrodes showed a uniform distribution of active materials over the Ag mesh current collectors. X-ray images of numerous Zn electrodes were recorded to assess the rate and extent of Zn material redistribution (shape change) that accompanied cell cycling. Figure 8 shows X-ray images of cells B1, L1 and C1 after the cells had completed the numbers of cycles indicated in the figure caption. All cells were examined in the discharged state, i.e. after discharging each cell to the 1.1 V cutoff voltage. Figure 8 shows, from left to right, Zn electrode #1, (a Zn electrode nearest to the cell container), Zn electrode #2, Zn electrode #3 and Zn electrode #4 (at the center of the cell pack). The cell shape-change patterns were symmetrical, i.e. the shape change pattern for Zn electrode #7 was similar to that of Zn electrode #1, the shape-change pattern of Zn electrode #6 was similar to that of Zn electrode #2, and so on. Cell B1 showed a modest extent of shape change after attaining 136 cycles. The LBL-cell group (L1 and C1) showed more extensive shape change, and the shape-change patterns were rather similar to one another. Three types of morphology can be easily distinguished in the electrodes of the LBL-group cells: (i) a dense, compact Zn area at the bottoms of the electrodes; (ii) 'islands' of zinc; (iii) areas of nearly bare current collector with a slight residual

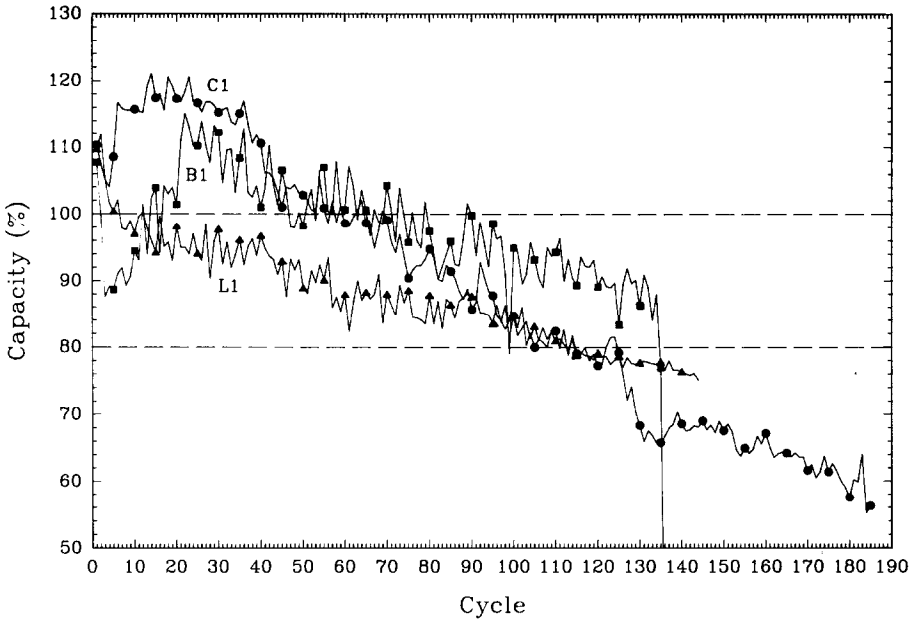

Fig. 6. Capacity vs cycle number for cells B1, L1 and C1. Electrolyte compositions are given in the legends of Figs. 2 and 3, and also in Table 2. B1 (■), L1 (▲) and C1 (●).

amount of Zn. The outermost Zn electrode (Zn electrode #1), which started cycling with half the capacity of its neighbors, exhibited mostly areas of nearly bare current collector and areas of dense, compact Zn. The island areas were more commonly found in the inner Zn electrodes (i.e., #2 through #6).

Other investigators (3–5) have shown that additions of Ca can reduce the rate and extent of Zn electrode shape change, particularly in electrolytes of low-to-moderate KOH concentration, because of the formation of a calcium zincate complex. Cell C1 exhibited extensive Zn electrode shape change, which leads one to suspect that the formation of the calcium zinc complex was inhibited by the high (45 wt.%) KOH concentration (this turns out not to be the case, see below). It appears to be more likely that the use of Dexter paper around the Zn electrodes in the BST cells inhibited the rate and extent of shape change, at least in 45 wt.% KOH electrolyte (see Fig. 8), compared to the LBL-cells which employed Celgard separator next to the Zn electrodes. Different types of Ag electrode current collectors were used in the LBL-group and BST-group cells (mesh and sheet, respectively), however it is less likely that this difference is the root cause of the dramatically different shape change patterns.

The three distinct areas of the various Zn electrode samples (nearly bare current collector, island, and dense areas) were examined microscopically using a SEM. This examination permits an assessment of the physical and chemical variations over microscopic areas of the electrodes. In cell B1 the uppermost area of the electrode (mainly bare current collector) exhibited needle-like metallic Zn on the surface, which led to the formation and growth of Zn dendrites. The lower area of the electrode contained typical porous Zn/ZnO material. Figures 9 and 10 show the morphologies of selected areas in Zn electrodes from cells L1 and C1, respectively. In cell L1 (Fig. 9), the island area contained porous Zn/ZnO material, and the bare current

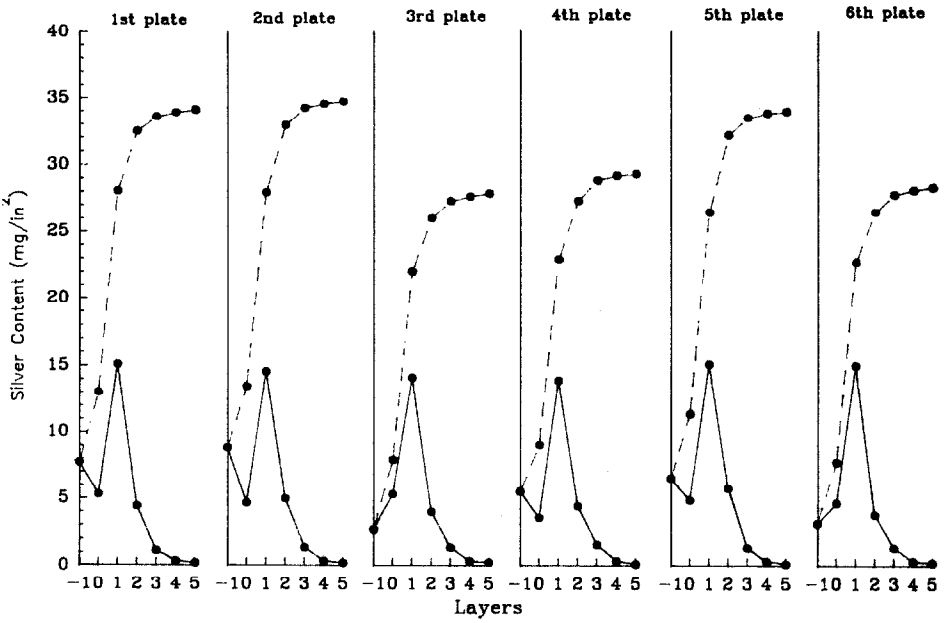

Fig. 7. Silver content in the separator system for cell C1 after 185 cycles. Abscissa designation: (−1) Pellon; (0) Celgard; (1, 2, 3, 4, 5) cellophane layers; (——) silver content in an individual layer; (– – –) cumulative silver content.

TABLE 3

Tensile strength[a] of cellophane

Sample condition	Breaking load (kg)
dry	2.1
wet	0.29
Hydrolysis conditions: 45% KOH + saturated ZnO and AgO at 90 °C	
24 h	0.22
48 h	0.10
72 h	0.03
Hydrolysis conditions: 39% KOH + 5% K_3BO_3 + saturated ZnO and AgO at 90 °C	
24 h	0.19
48 h	0.05
Hydrolysis conditions: 38% KOH + 8% K_2CO_3 + saturated ZnO and AgO at 90 °C	
24 h	0.17

[a]Loading speed = 10 cm/min.
Loading sample = 10 cm × 0.95 cm.

collector and dense areas contained very compact material (Figs. 9a and 9c), however some of the material in these areas has a porosity similar to that of the island area. In cell C1 (Fig. 10), all three areas exhibited crystals typical of the calcium zincate complex. In particular, the island area (Fig. 10b) contained large amounts of these tetragonal crystals. The bare current collector and dense areas (Fig. 10a and 10c)

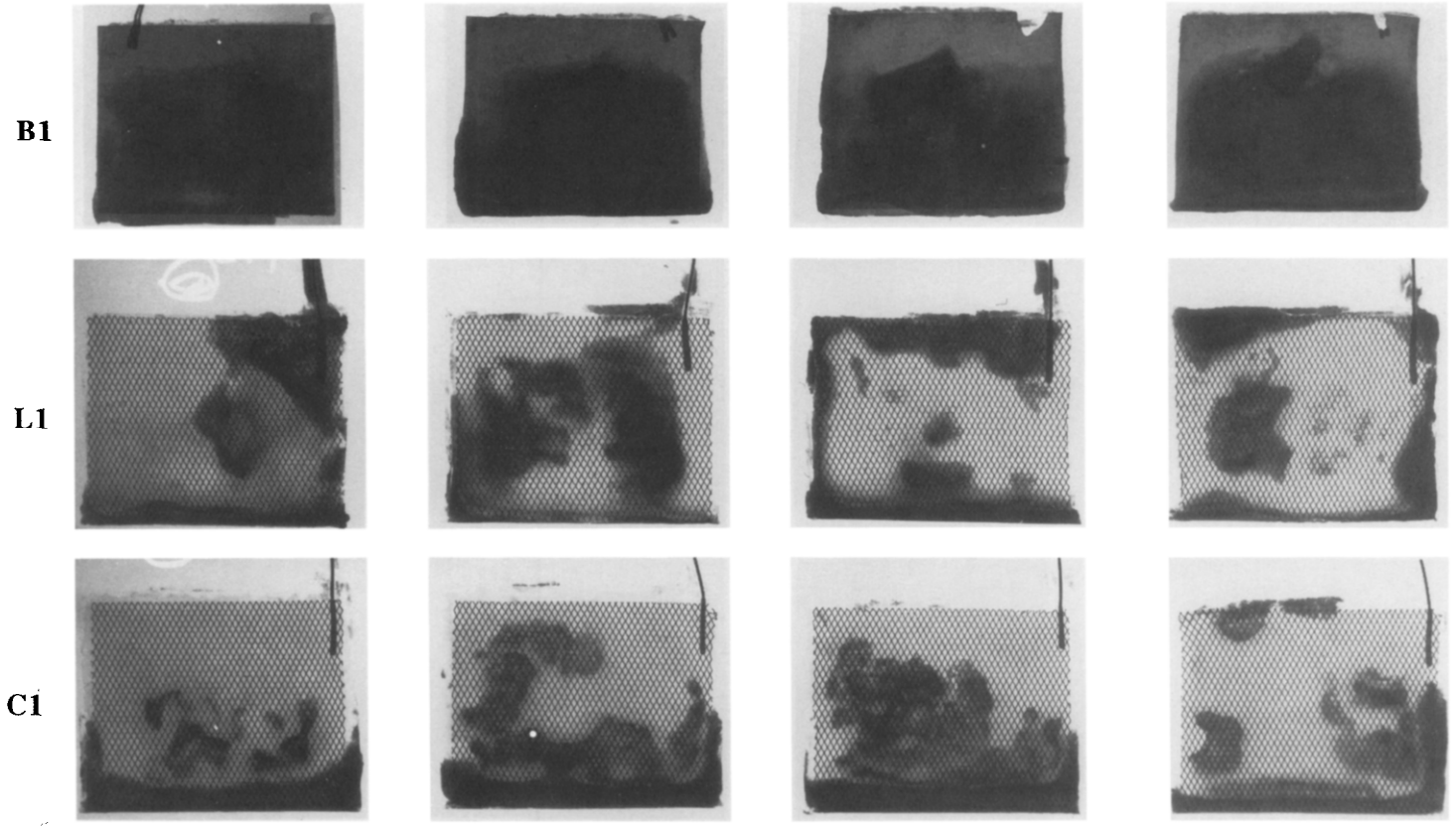

Fig. 8. X-ray photographs of representative Zn electrodes harvested from cells B1 (136 cycles), L1 (145 cycles) and C1 (185 cycles), respectively, shown from top to bottom. From left to right, the images are those of Zn electrode #1 (an electrode nearest to the cell case), Zn electrode #2, Zn electrode #3, and Zn electrode #4 (located at the center of the cell pack). Similar shape-change patterns were seen on the corresponding Zn electrodes harvested from the opposite halves of each cell, i.e. Zn electrodes #5, #6 and #7.

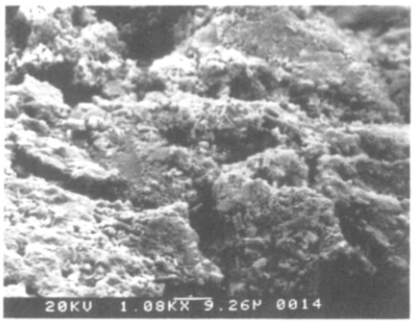

(a)

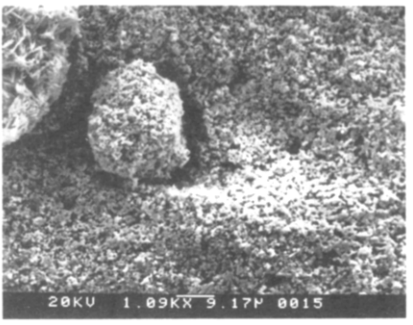

(b)

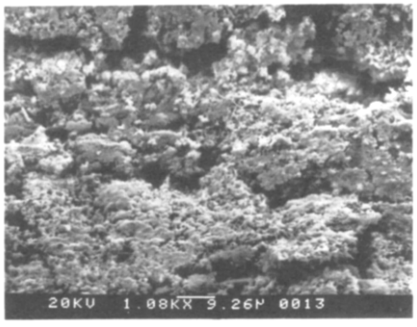

(c)

Fig. 9. Morphology of active material in selected areas of a Zn electrode harvested from cell L1; (a) mainly bare current collector with slight residual Zn area; (b) island area, and (c) dense area.

contained fewer tetragonal crystals, and in the dense area hexagonal crystals were found. Obviously, the morphology of Zn–Ca electrodes differs dramatically from that of the typical Zn electrode, and the use of 45 wt.% KOH electrolyte does not prevent the formation of calcium zincate crystals. The good cycle-life performance of cell C1 may be attributed the formation of the calcium zinc complex, however the great extent of shape change suggests that even better performance could be realized, perhaps by improving the wetting characteristics of the electrode.

Table 2 lists cycle-life performance data for the three groups of 5 A h Zn/AgO cells that were cycled. Included in this table are values of the capacity loss rate (expressed as %/cycle, based on the initial cell capacity) and the average delivered capacity per cycle, both based on the cell performance before its capacity dropped to 4.0 A h. These 'figures of merit' illustrate the superior cycle-life performance of the calcium-containing Zn/AgO cells.

Conclusions

1. The ability of reduced-zinc-solubility electrolytes, prepared by adding F^-, CO_3^{2-}, BO_3^{3-} and PO_4^{3-} to KOH electrolyte, to extend the cycle life of Zn/AgO cells was

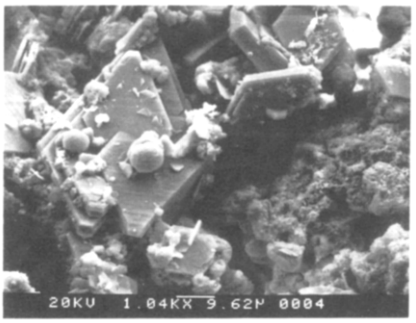

(a)

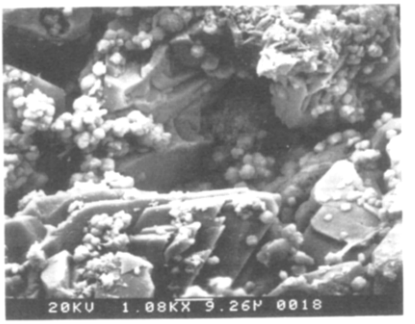

(b)

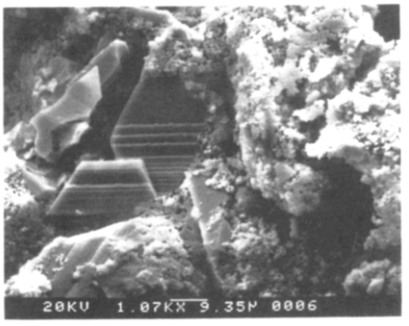

(c)

Fig. 10. Morphology of active material in selected areas of a Zn–Ca electrode harvested from cell C1; (a) mainly bare current collector with slight residual Zn area; (b) island area, and (c) dense area.

examined. It would appear that all of the anion additives to KOH electrolytes result in lower capacities. Lower capacities can be attributed to poor Ag electrode behavior, which could be due to the formation of inorganic salts, e.g., AgF, AgF_2, Ag_2CO_3, Ag_2BO_3 and Ag_3PO_4, that cause active materials loss.

2. The calcium-containing zinc electrode was found to significantly improve the performance of the Zn/AgO cell by promoting higher capacities, especially over the initial 20 cycles. The higher capacities can be attributed to the formation of a calcium zincate complex, crystals of which were found in the cycled zinc electrodes. This result bears further investigation.

3. In the analysis of the Ag content of the separator, results showed that the Ag content became progressively smaller through a single layer of Pellon and Celgard and three layers of cellophane. Cellophane was a good material to prevent Ag penetration. The results of separator tensile-strength measurements showed that the tensile strength of cellophane decreased with lower KOH concentration.

4. Because $Ca(OH)_2$ is a beneficial additive to the Zn electrode in Zn/AgO cells, it is suggested that further research focus on investigations of Zn–Ca/AgO cells to better understand the mechanism whereby the capacity improvements are realized, the development of Zn–Ca/AgO cells with improved wetting characteristics, the fabrication of sealed Zn–Ca/AgO cells, and characterization of large Zn–Ca/AgO cells

Acknowledgements

BST, Inc. provided several Zn/AgO cells, electrodes and cell parts, the authors wish to thank BST for providing these useful materials. The experimental and analytical help provided by Mr Thomas Adler and Dr Kathryn Striebel is gratefully acknowledged.

This work was supported by the Defense Advanced Research Projects Agency, Undersea Warfare Office, Submarine Technology Program, under ARPA Order Number MIPR N0002490MP70004 with the Lawrence Berkeley Laboratory.

References

1 S. F. Schiffer, in *Handbook of Batteries & Fuel Cells,* D. Linden (ed.), McGraw-Hill, New York, 1984, Ch. 21.
2 A. Himy, in *Silver–Zinc Battery–Phenomena and Design Principles,* Vantage Press, New York, 1986.
3 F. R. McLarnon and E. J. Cairns, *J. Electrochem. Soc., 138* (1981) 645.
4 E. G. Gagnon, *J. Electrochem. Soc., 133* (1986) 1989.
5 R. Jain, F. R. McLarnon and E. J. Cairns, *Lawrence Berkeley Laboratory Report, No. LBL-25332,* 1989.
6 E. G. Gagnon and R. A. Sharma, *J. Electrochem. Soc., 133* (1986) 2215.
7 J. T. Nichols, F. R. McLarnon and E. J. Cairns, *Lawrence Berkeley Laboratory Report, No. 17397,* 1983.
8 M. H. Katz, J. T. Nichols, F. R. McLarnon and E. J. Cairns, *J. Power Sources, 10* (1983) 149.
9 D. A. Skoog, D. M. West and F. J. Holler, in *Fundamentals of Analytical Chemistry,* Saunders College Publishing, New York, 1988.
10 Y.-M. Wang, *J. Electrochem. Soc., 137* (1990) 2800.
11 T. P. Dirkse, *J. Electrochem. Soc., 106* (1959) 453.
12 A. Fleicher and J. J. Lander (eds.), in *Zinc–Silver Oxide Batteries,* Wiley Interscience, New York, 1971, p. 136.